BIOMECHANICS

How flight feathers stick together to form a continuous morphing wing

Laura Y. Matloff[1], Eric Chang[1], Teresa J. Feo[2,3], Lindsie Jeffries[1], Amanda K. Stowers[1], Cole Thomson[1], David Lentink[1]*

Variable feather overlap enables birds to morph their wings, unlike aircraft. They accomplish this feat by means of elastic compliance of connective tissue, which passively redistributes the overlapping flight feathers when the skeleton moves to morph the wing planform. Distinctive microstructures form "directional Velcro," such that when adjacent feathers slide apart during extension, thousands of lobate cilia on the underlapping feathers lock probabilistically with hooked rami of overlapping feathers to prevent gaps. These structures unlock automatically during flexion. Using a feathered biohybrid aerial robot, we demonstrate how both passive mechanisms make morphing wings robust to turbulence. We found that the hooked microstructures fasten feathers across bird species except silent fliers, whose feathers also lack the associated Velcro-like noise. These findings could inspire innovative directional fasteners and morphing aircraft.

Bird flight feathers are hierarchically organized down to the micrometer scale (*1*–*6*), which makes them both firm enough to sustain lift and soft enough to smoothly overlap with adjacent feathers. Variable feather overlap enables birds to morph their wing and tail planforms more extensively than insects, bats (*7*), and current aircraft (*8*, *9*), providing unparalleled flight control (*10*, *11*); yet, how feather motion is coordinated during wing extension and flexion is not fully understood (*12*, *13*). Previous researchers hypothesized that flight feather coordination could be facilitated in several ways. A morphological study in pigeons (*13*) suggests that the smooth muscles and ligaments interconnecting the remiges may provide passive guidance for feather coordination. Feather microstructures termed "friction barbules" may prevent overlapping feathers from sliding too far apart during wing extension (*14*–*18*), but the mechanism responsible is unclear. Graham (*14*, *19*) suggested that the microscopic hooks of friction barbules may fasten adjacent feathers together by increasing friction, whereas subsequent work (*3*, *15*–*18*, *20*) suggested that they simply increase friction between feathers. Fastening and friction have different implications for our understanding of the evolution of avian flight. For instance, fastening during wing extension requires a mechanism to unfasten during flexion. On the other hand, "the energetic costs to overcome frictional forces during wing extension and flexion would be extremely large" (*12*).

To quantify how flight feathers are coordinated passively by means of elastic tissue between the base of the feathers, we measured the skeletal and flight feather kinematics of a rock pigeon (*Columba livia*) wing morphing between different glide poses (*21*, *22*) (Fig. 1, A and B; see methods). We found that feathers are redistributed through near-linear transfer functions that map the input wrist angle to each feather angle (Fig. 1, C and D). The slope represents the sensitivity of feather angle to wrist angle, and differences in slopes between adjacent feathers indicate how closely the motion of adjacent feathers is coupled (Fig. 1E). This shows how a series of tuned elastic ligaments between the remiges (the postpatagium) couples the wrist angle to all 20 remex angles (Fig. 1F). This 20:1 reduction in the number of degrees of freedom is classified as an underactuated mechanism in robotics, which formalizes earlier anatomical observations (*13*). However, it may not be entirely passive in vivo. Smooth muscles connecting the remiges may tune the stiffness of the underactuated mechanism (*13*), albeit not within a wingbeat cycle, because smooth muscles contract orders of magnitude more slowly (*23*, *24*). Although the corroborated elastic underactuation explains how feathers are distributed, it does not explain how gaps between feathers are prevented during wing extension.

When separating two overlapping pigeon flight feathers by hand, they initially slide smoothly before suddenly locking in place, suggesting that there must be a micromechanical end stop. To investigate this, we pressed the vane surfaces together with a predefined

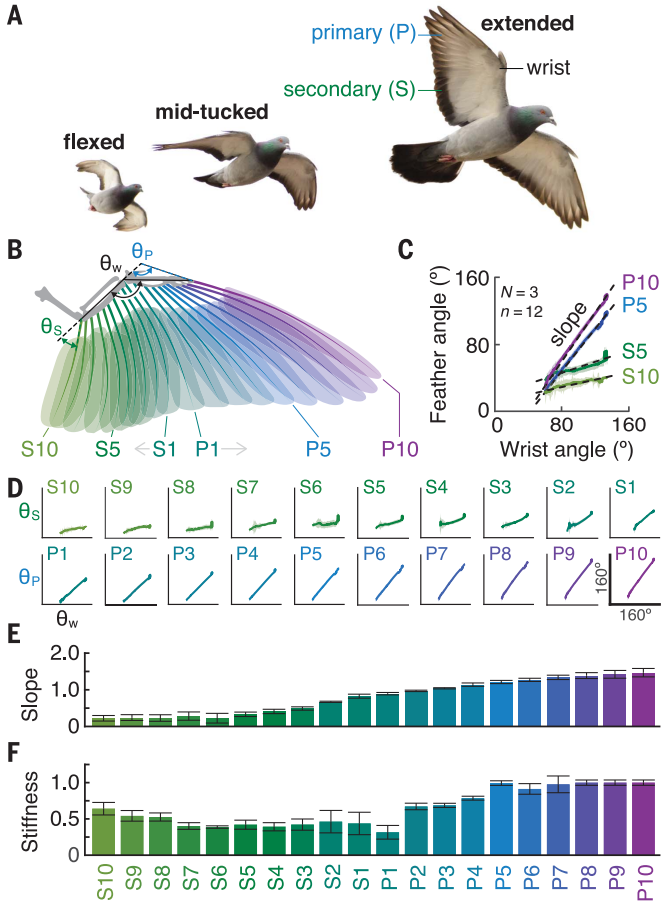

Fig. 1. Pigeon flight feathers are underactuated during wing flexion and extension. (**A**) Birds morph their wings during flight by flexing and extending their skeleton. (**B**) During morphing, as the wrist angle (θ_w) extends, flight feathers pivot relative to the ulna bone, measured by primary and secondary feather angles (θ_P and θ_S). (**C**) Linear transfer functions model the relationship between the wrist angle and feather angle. *N*, individuals; *n*, cycles each. (**D**) Measurements of all feather angles follow a linear relationship to wrist angle, suggesting underactuation. (**E**) The slopes of the linear model represent the sensitivity of the feather angles to wrist angle. (**F**) A linear elastic spring model corroborated from the feather transfer functions yields the normalized spring stiffness distribution of the connective tissue between the remiges. Error bars represent standard deviation.

[1]Department of Mechanical Engineering, Stanford University, Stanford, CA, USA. [2]Department of Vertebrate Zoology, National Museum of Natural History, Smithsonian Institution, Washington, DC, USA. [3]California Council on Science and Technology, Sacramento, CA, USA.
*Corresponding author. Email: dlentink@stanford.edu

normal force and then slowly rotated away the overlapping feather about the calamus tip using a computer-controlled motor. Simultaneously, we measured the time-resolved normal and opposing forces between the separating feathers (fig. S1 and methods). Across primary remiges (P10 and P9; P6 and P5), secondary remiges (S5 and S6), and rectrices (R5 and R6), we measured that flight feathers first slide with low opposing forces before they lock, causing the feathers to resist separation and the vanes to deform as a result (Fig. 2A). In the locked state, the force reaches a maximum, but because the feathers are forced to continue sliding, unfastening and refastening dynamically, they fail catastrophically (fig. S17 and movie S1) and separate (Fig. 2A). Simulating both wing flexion and extension, we observed that the opposing force is directional in pigeons: The maximum opposing force during extension is up to 10 times higher than during flexion (Fig. 2B). As a control, we slid the feather vanes along the rachis directions (anterior and posterior) and found low opposing forces similar to those in flexion. We evaluated the effect of normal force on the separation force as predicted by Coulomb's friction law: friction force = friction coefficient × normal force (Fig. 2C). A micrometer stage varied normal force by pressing feathers together from 50 mN

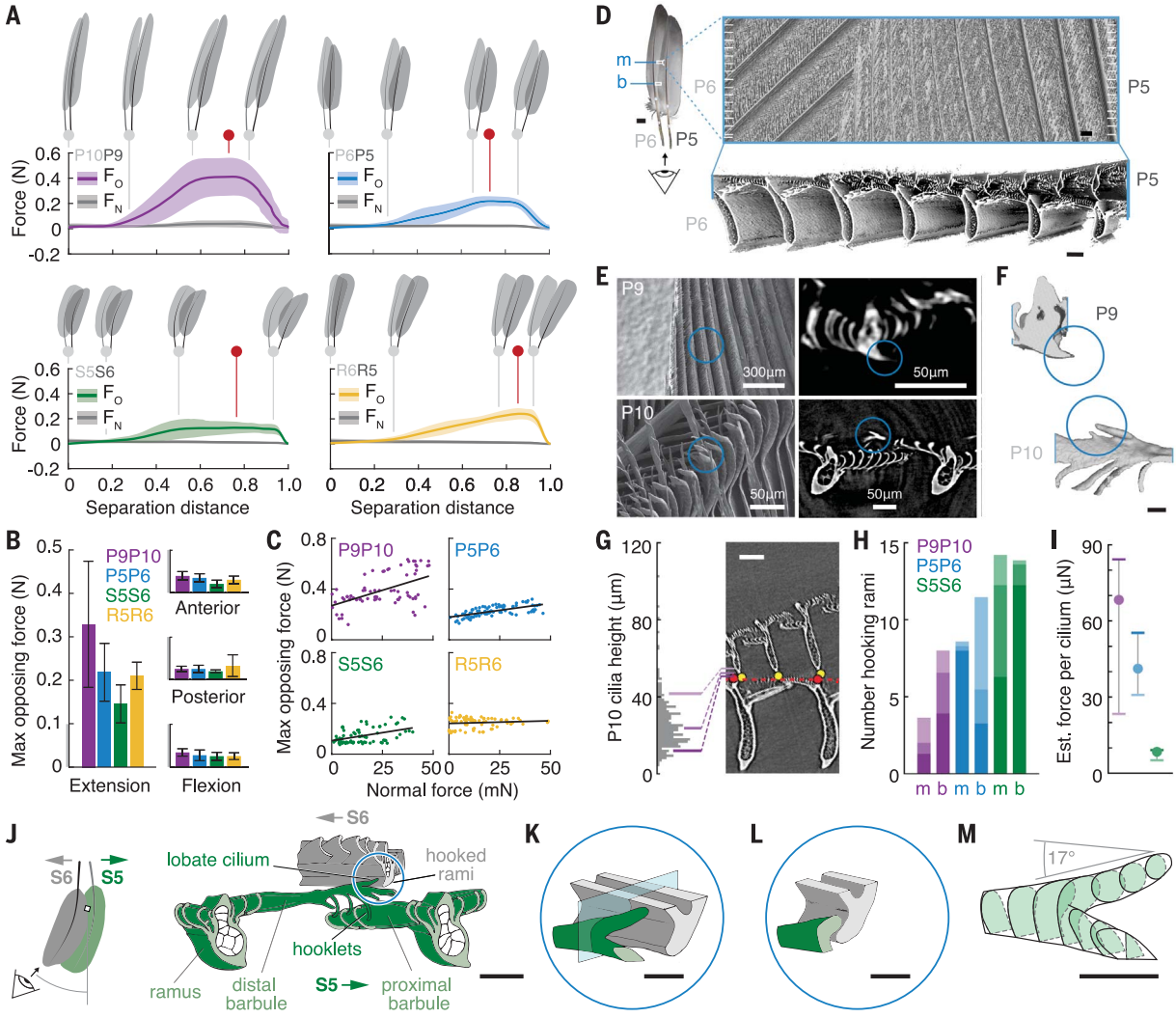

Fig. 2. Pigeon flight feathers lock together by means of microscopic directional probabilistic fasteners. (**A**) The opposing force (F_O) between pigeon flight feather pairs starts low and then ramps up before separation, whereas the normal force (F_N) remains low throughout (red pin indicates max force; values are averaged across normal force levels; feather outlines are from movie S1; shaded regions indicate force standard deviation). R, rectrix. (**B**) Maximal opposing forces are up to 10 times higher in the extension direction than in the flexion, posterior, and anterior directions. Error bars represent standard deviation. (**C**) Maximum opposing forces weakly depend on normal force and lack an intercept at zero. (**D**) Micro-CT scans of the overlapping feather pair P6-P5 show how their surfaces engage [scale bars are 10 mm (left) and 100 μm (top right and bottom right)]. See movie S2. m, middle; b, base. (**E** and **F**) Scanning electron microscopy images [(E), left], beamline micro-CT cross sections [(E), right], and three-dimensional reconstructions [(F); scale bar, 10 μm] of the microstructures (blue circles) involved in directional fastening. Top row: P9 overlapping outer vane rami with hook-shaped ventral ridge. Bottom row: P10 underlapping inner vane barbules with hooklike lobate dorsal cilia. (**G** and **H**) The distribution of lobate cilia protrusion height (G) was used to calculate the number of rami (yellow dots) hooked with cilia (beyond red dashed line; see methods for details) along vane-wise cross sections [white tick marks in (D)] (H). (**I**) Estimated force per hooked lobate cilium (see methods). Error bars represent standard deviation. (**J**) The interaction between a single lobate cilium and hooked ramus, as viewed from the feather tip (movie S3; scale bar, 50 μm). (**K** to **M**) The lobate cilium nestles snugly against the hooked ramus (L) via the sideward hooked lobe (M) after the slanted tip directs the ramus in position (scale bars, 10 μm; 17° is the angle for this lobate cilium).

down to as little as 0.2 mN (the sensor resolution limit). Even for the smallest normal forces, flight feathers locked in place with measured opposing forces close to 0.2 N (Fig. 2C and fig. S17). This large force, $^{1}/_{25}$ of body weight, is of the same order of magnitude as the lift that each flight feather has to support in gliding flight (body weight/40 remiges that form the wings). Coulomb friction requires unusually high friction coefficients, greater than 1000 for a normal force of 0.2 mN, well beyond established material properties (*25*). Furthermore, locking forces vary little with normal force and lack the intercept at zero normal force, which rules out Coulomb friction.

The distinctive interfeather fastener characteristics emerge from their hierarchical organization down to the microscale, which we visualized through scanning electron and x-ray microscopy (movies S2 and S3). Locking occurs in a spread wing or tail when the downward-curved outer vane of an overlapping flight feather slides across the upward-curved inner vane of an underlapping flight feather, in which the opposed curvatures ensure that the vane surfaces mate (*18*). In this region (Fig. 2D; see fig. S2 for nomenclature), the underlapping inner vanes have modified distal barbules with enlarged, hooked, lobate, dorsal cilia that extend above the dorsal ridge of the rami (Fig. 2E, bottom row; see figs. S3 to S6 for distributions). The overlapping outer vanes have rami with hook-shaped ventral ridges (Fig. 2E, top row, and figs. S9 and S10). To characterize the fastening mechanism between a hooked rami and single lobate cilium, we first estimated the number of locked lobate cilia in a feather pair (Fig. 2, G and H; fig. S12; and methods). The calculated maximum force per cilium is 10 to 70 μN (Fig. 2I), equivalent to the ~14 μN per hooklet (*4*) that zips barbs in the vane together (*3*, *4*, *6*). Notably, the same distal barbule functions both to fasten barbs within a flight feather by means of ventral hooklets and to fasten flight feathers within a wing by means of dorsal lobate cilia (Fig. 2J and fig. S13). The hooklets are oriented along the distal barbule to connect to proximal barbules, whereas the principal hooking direction of the lobate cilium is oriented to the side (Fig. 2, J to M, and fig. S11) to align with the hooked rami of the overlapping feather (figs. S7 and S8). Consequently, the principal hooking directions of the interbarb and interfeather fasteners are roughly orthogonal (Fig. 2J, fig. S13, and movie S3) and are thus functionally decoupled. The sophistication of the lobate cilium hooking mechanism culminates in its upward slanted tip sticking out above the rami (Fig. 2M and fig. S11). This enables the lobate cilium to catch and direct the overlapping hooked ramus so that its hooked lobe ends up nestling snug against the hooked ramus (Fig. 2, K and L, and movie S3), securely fastening both feathers during extension and automatically unlocking them during flexion. Fastening contradicts the hypothesized enhanced friction function of friction barbules (*3*, *12*, *14*–*20*), which we rename "fastening barbules" accordingly. This clarifies the function of the thousands of fastening barbules on the underlapping flight feathers; they lock probabilistically with the tens to hundreds of hooked rami of the overlapping flight feather and form a feather-separation end stop. The emergent properties of the interfeather fastener are not only probabilistic like bur fruit hooks, which inspired Velcro, but also highly directional like gecko feet setae (*26*)—a combination that has not been observed before (*27*).

To evaluate the function of both interfeather directional fastening and passive elastic feather redistribution on feather coordination in flight, we created a new biohybrid aerial robot with 40 underactuated pigeon remiges (Fig. 3A). We found that both underactuation and directional fastening are required to passively coordinate feather motion during dynamic wing morphing under calm outdoor flight as well as extremely turbulent conditions. Flight tests (Fig. 3B, fig. S14, and movie S4) demonstrated that the biohybrid wing morphs reliably at high flexion and extension frequencies of ~5 Hz, representative for pigeons (*21*). To quantitatively probe the function of passive elastic ligaments and interfeather directional fastening, we tested the robot wing at its approximate cruising speed (~10 m/s) and angle of attack (~10°) in a variable-turbulence wind tunnel. We manipulated the robot wing in four configurations in which we permutated removing the elastic ligaments and rotating the feathers along the rachis to separate the vanes (see methods). Tests in both high turbulence (30%; Fig. 3C) and low turbulence (3%; fig. S15) showed that elastic underactuation and feather fastening are required for continuous morphing. Without feather contact, but with elastic ligaments, gaps form between the primary feathers (Fig. 3D). Without elastic ligaments, but with feather contact, even larger gaps form as feathers move together in clumps (Fig. 3E). The wing without either elastic ligaments or feather contact has no coherent

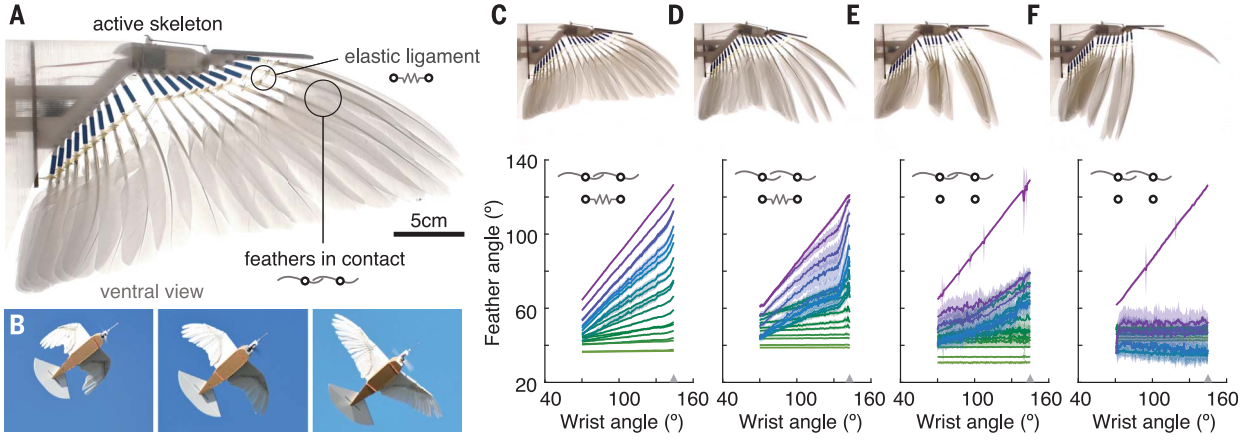

Fig. 3. Underactuated remiges with directional probabilistic fasteners morph robustly in flight. (**A**) We developed a biohybrid robotic wing with active skeletal control and 20 underactuated pigeon remiges in each wing half to evaluate the function of passive elastic ligaments and probabilistic directional fastening of adjacent feathers during dynamic wing morphing. (**B**) Successful outdoor flight of the biohybrid robot, demonstrating fully tucked, mid-tucked, and fully extended wings (movie S4). (**C** to **F**) Wind tunnel testing of the biohybrid wing in high turbulence (movie S5) with elastic coupling [(C) and (D)] and feather contact [(C) and (E)]. Both elastic coupling and feather contact (C) are required to maintain a continuous planform during wing morphing, whereas all other conditions [(D) to (F)] result in unnatural separation of the feathers and gaps in the planform. Note that the outermost feather P10 and the innermost feather S10 are fixed to the skeleton (for low turbulence, see fig. S15). Views are of the underside of the wing. Color scheme is the same as in Fig. 1B.

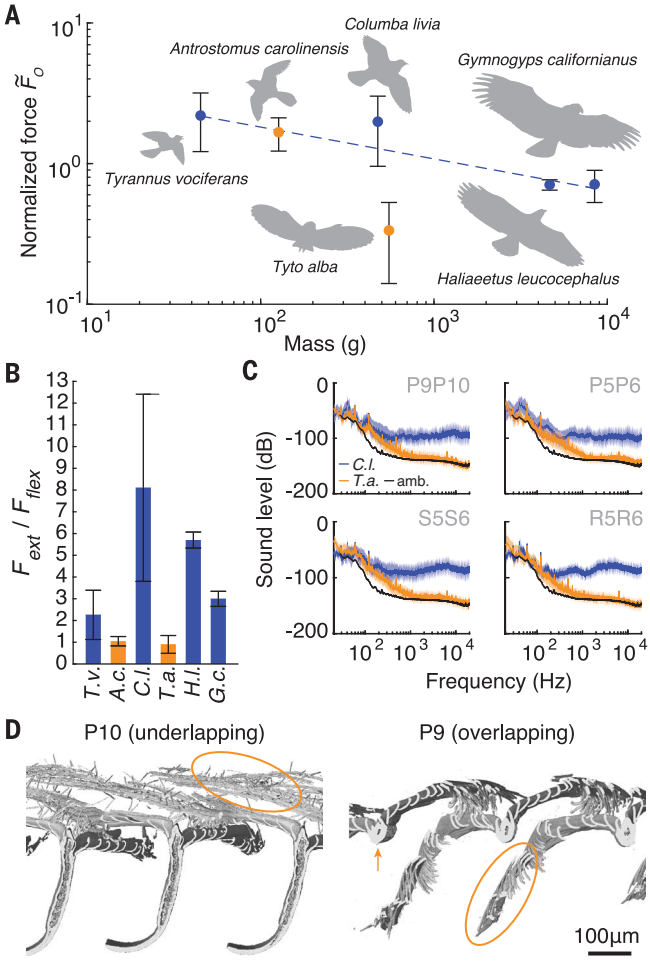

Fig. 4. Scaling and specialization of probabilistic feather fasteners across species. (**A**) Measured opposing feather-locking forces normalized by the nominal aerodynamic loading of each flight feather [$\tilde{F}_O = F_O$/(body weight/number of remiges)] for bird species ranging from ~40 g (Cassin's kingbird, *Tyrannus vociferans*) to ~9000 g (California condor, *Gymnogyps californianus*) (table S2). The trendline (blue dashed line) is shown with silent-flight species (orange) omitted. Silhouettes are based on fieldbook illustrations (*30*). Error bars represent standard deviation. (**B**) Extension-to-flexion ratios of opposing force (F_{ext} and F_{flex}) show that feather forces are directional, except for the species specialized in silent flight: barn owl (*T.a.*, *Tyto alba*) and chuck-will's-widow (*A.c.*, *Antrostomus carolinensis*). *T.v.*, *T. vociferans*; *C.l.*, *C. livia*; *H.l.*, *Haliaeetus leucocephalus*; *G.c.*, *G. californianus*. Error bars represent standard deviation. (**C**) Feather separation is much noisier in pigeon feathers than in owl feathers (movie S6). Shaded regions indicate standard deviation. amb., ambient noise level. (**D**) Beamline micro-CT scan of barn owl feathers shows the lack of lobate dorsal cilia in the inner vane of underlapping P10 and the lack of a hooked ventral ridge (orange arrow) in the outer vane rami of overlapping P9. Instead, both P10 distal barbules and P9 proximal barbules have elongated pennulae (~3-µm-diameter elongated structures in orange ellipses) that project beyond the plane of the rami.

feather coordination (Fig. 3F). In both outdoor flights and wind tunnel experiments, we consistently observed that directional fastening prevents gaps in the wing planform by locking adjacent remiges that risk separation, whereas elastic underactuation redistributes the locking forces to move unlocked remiges in place. Remiges only lock simultaneously during extreme wing extension, when feather sliding velocities approach zero (fig. S16), which minimizes the rate of energy loss (force × sliding velocity). Finally, the strong directionality in the locking force ensures that wing flexion is not resisted.

The directional probabilistic fastening mechanism between adjacent flight feathers is present across a wide range of modern bird species on the basis of three independent lines of evidence. First, the lobate dorsal cilia that enable fastening have been described across a wide range of species (*28*) (table S4). Second, we qualitatively observed interfeather fastening forces across a diverse set of species, except for silent flyers such as owls (table S3 and methods). Finally, we directly measured the interfeather fastening forces across select bird species ranging in body mass from a ~40-g Cassin's kingbird to a ~9000-g California condor (Fig. 4, A and B). The maximum measured force normalized by the estimated aerodynamic loading of each flight feather (body weight/number of remiges) has an order of magnitude of one across birds and scales only weakly with mass (mass$^{-0.2}$; Fig. 4A). Consequently, feather fastening forces are a similar fraction of body weight, and thus similarly effective, in both small and big birds. The fastening force is directional, with a force ratio of at least two between extension versus flexion across this range (Fig. 4B), except for the silent fliers (barn owl and chuck-will's-widow; Fig. 4B and table S3). High-resolution computerized tomography (CT) scans of barn owl feathers show that they indeed lack the lobate cilia and hooked rami in regions of feather overlap and instead have modified barbules with elongated, thin, velvety pennualue (Fig. 4D). This explains the low friction-like opposing forces we measured between their feathers (figs. S18A and S19A). Indeed, completely separating overlapping pairs of pigeon feathers produces a Velcro-like broadband sound, whereas separating barn owl flight feathers produces comparatively little noise, roughly 40 dB lower at 1 kHz (Fig. 4C, fig. S20, and methods). This confirms a functional tradeoff between feather fastening and sound dampening (Fig. 4C), which Graham noted (*19*), and may explain the evolutionary loss of fastening barbules in species under selection for silent flight. We hypothesize that directional fastening may not be as critical for some silent fliers because decaying atmospheric turbulence at night (*29*) reduces the risk of feather slipping. The evolution of fastening barbules thus represents an important functional innovation in the transition from feathered dinosaurs to modern birds, which fossils may shed light on.

REFERENCES AND NOTES

1. R. O. Prum, *J. Exp. Zool.* **285**, 291–306 (1999).
2. M. Yu, P. Wu, R. B. Widelitz, C.-M. Chuong, *Nature* **420**, 308–312 (2002).
3. A. M. Lucas, P. R. Stettenheim, *Avian Anatomy: Integument Part I and Part II* (U.S. Government Printing Office, 1972).
4. A. Kovalev, A. E. Filippov, S. N. Gorb, *J. R. Soc. Interface* **11**, 20130988 (2013).
5. T. N. Sullivan *et al.*, *Adv. Funct. Mater.* **27**, 1702954 (2017).
6. F. Zhang, L. Jiang, S. Wang, *Proc. Natl. Acad. Sci. U.S.A.* **115**, 10046–10051 (2018).
7. C. J. Pennycuick, *Modelling the Flying Bird* (Elsevier, 2008).
8. S. Barbarino, O. Bilgen, R. M. Ajaj, M. I. Friswell, D. J. Inman, *J. Intell. Mater. Syst. Struct.* **22**, 823–877 (2011).
9. D. D. Chin, L. Y. Matloff, A. K. Stowers, E. R. Tucci, D. Lentink, *J. R. Soc. Interface* **14**, 20170240 (2017).
10. D. Lentink *et al.*, *Nature* **446**, 1082–1085 (2007).
11. K. E. Crandell, B. W. Tobalske, *J. Exp. Biol.* **214**, 1867–1873 (2011).
12. J. J. Videler, *Avian Flight* (Oxford Univ. Press, 2006).
13. T. L. Hieronymus, *J. Anat.* **229**, 631–656 (2016).
14. R. R. Graham, *J. R. Aeronaut. Soc.* **36**, 24–58 (1932).
15. H. Sick, *J. Ornithol.* **85**, 206–372 (1937).
16. E. Rutschke, *J. Ornithol.* **106**, 307–312 (1965).
17. H. Oehme, *J. Ornithol.* **100**, 363–396 (1959).
18. H. Oehme, *Biol. Zent. Bl.* **82**, 569–587 (1963).
19. R. R. Graham, *Aeronaut. J.* **38**, 837–843 (1934).
20. N. S. Proctor, P. J. Lynch, *Manual of Ornithology: Avian Structure and Function* (Yale Univ. Press, 1993).
21. C. J. Pennycuick, *J. Exp. Biol.* **49**, 527–555 (1968).
22. A. K. Stowers, L. Y. Matloff, D. Lentink, *J. R. Soc. Interface* **14**, 20170224 (2017).
23. B. B. Hafen, B. Burns, in *Anatomy* (StatPearls Publishing, 2018); www.ncbi.nlm.nih.gov/books/NBK532857/.
24. J. C. Rüegg, *Physiol. Rev.* **51**, 201–248 (1971).

25. D. E. Gray, *American Institute of Physics Handbook* (McGraw-Hill Book Company Inc., 1957), section 2d.
26. K. Autumn *et al*., *Nature* **405**, 681–685 (2000).
27. S. N. Gorb, in *Springer Handbook of Nanotechnology*, B. Bhushan, Ed. (Springer, 2010), pp. 1525–1551.
28. A. C. Chandler, *A Study of the Structure of Feathers: With Reference to Their Taxonomic Significance* (Univ. California Press, 1916), vol. 13.
29. R. B. Stull, *An Introduction to Boundary Layer Meteorology* (Springer, 2012), vol. 13.
30. C. S. Robbins, B. Bruun, H. S. Zim, A. Singer, *Birds of North America: A Guide to Field Identification* (Golden Books Publishing Company Inc., 1983).
31. L. Y. Matloff, E. Chang, T. J. Feo, L. Jeffries, A. K. Stowers, C. Thomson, D. Lentink, How flight feathers stick together to form a continuous morphing wing online data. Figshare (2019); http://dx.doi.org/10.6084/m9.figshare.11369364.

ACKNOWLEDGMENTS

We thank A. Engilis and I. E. Engilis for feather loans; A. Vailiones for CT scanning help with NSF ECCS-1542152 support; K. Rogers (CDFW), K. Miller, and E. I. Knudsen for owl cadavers; J. Kadis, C. Basica, E. Georgieva, and B. Hightower for sound recording help; G. W. Reich for AFOSR flight permit support; and R. Prum for beamline 2-BM CT scanning of feathers with T.J.F. at Argonne National Laboratory (U.S. Department of Energy proposal 41887 to R. Prum) and analysis, with help of X. Xiao, S. Whittaker, C. Dove, and H. James for SEM support at the Smithsonian National Museum of Natural History. **Funding:** This project was supported by AFOSR BRI award number FA9550-16-1-0182 and AFOSR DESI award number FA9550-18-1-0525, with special thanks to B. L. Lee, F. A. Leve, and J. L. Cambier leading the program. T.J.F. was supported by NSF PRFB 1523857. E.C. and L.J. were supported by a NSF GRFP fellowship, A.K.S. by a NDSEG fellowship, and D.L. by NSF CAREER award 1552419. **Author contributions:** All authors contributed to the conception and design of the study and data analysis. D.L., L.Y.M., T.J.F., and E.C. wrote the manuscript; L.Y.M., E.C., T.J.F., L.J., and D.L. made the figures; L.Y.M. and A.K.S. performed motion capture; L.Y.M. made the spring model; L.Y.M. and C.T. performed feather interaction force measurements; T.J.F. performed scanning electron microscopy and beamline micro-CT imaging and analysis; L.J. performed micro-CT imaging of feather interaction; L.J., L.Y.M., and E.C. estimated force per cilium; E.C. fabricated the robot body; A.K.S., L.Y.M., and E.C. iterated and fabricated biohybrid robot wings; E.C. and L.Y.M. performed wind tunnel tests; E.C., L.Y.M., and A.K.S. performed flight tests; L.Y.M. and E.C. performed feather sound measurements; and D.L. contributed advice and supervised the work. **Competing interests:** The authors declare no competing interests. **Data and materials availability:** All data are available in the main text or the supplementary materials, as well as online at figshare (*31*).

SUPPLEMENTARY MATERIALS

science.sciencemag.org/content/367/6475/293/suppl/DC1
Materials and Methods
Figs. S1 to S20
Tables S1 to S4
References (*32*–*37*)
Movies S1 to S6

31 August 2019; accepted 18 December 2019
10.1126/science.aaz3358

How flight feathers stick together to form a continuous morphing wing

Laura Y. Matloff, Eric Chang, Teresa J. Feo, Lindsie Jeffries, Amanda K. Stowers, Cole Thomson and David Lentink

Science **367** (6475), 293-297.
DOI: 10.1126/science.aaz3358

Wing shapes take flight

Birds can dynamically alter the shape of their wings during flight, although how this is accomplished is poorly understood. Matloff *et al.* found that two mechanisms control the movement of the individual feathers. Whenever the skeleton moves, the feathers are redistributed passively through compliance of the elastic connective tissue at the feather base. To prevent the feathers from spreading too far apart, hook-shaped microstructures on adjacent feathers form a directional fastener that locks adjacent feathers. These features are found across a range of bird sizes; however, because the detachment of the hooks is noisy, they are notably absent in silent fliers, such as barn owls.

Science, this issue p. 293